JOURNAL OF GEOPHYSICAL RESEARCH, VOL. 97, NO. A7, PAGES 10,513–10,524, JULY 1, 1992

Comparison of Measured and Modeled Solar EUV Flux and its Effect on the *E-F1* Region Ionosphere

M. J. BUONSANTO

Haystack Observatory, Massachusetts Institute of Technology, Westford

S. C. SOLOMON

Laboratory for Atmospheric and Space Physics, University of Colorado, Boulder

W. K. TOBISKA[1]

Space Sciences Laboratory, University of California, Berkeley

The response of the *E-F1* region ionosphere to different solar EUV flux models is investigated theoretically using two different photochemical schemes, and the results are compared with incoherent scatter radar electron density measurements taken at Millstone Hill. The latest EUV flux model (Tobiska, 1991), which incorporates more recent measurements, has generally more flux at short wavelengths compared to the Hinteregger et al. (1981) flux model based on AE-E satellite data. This results in better agreement with the measurements in the *E-F1* region and above. The Tobiska flux model, however, gives a smaller E' region peak density, due to the influence of low Lyman β flux in the November 10, 1988, rocket measurements of Woods and Rottman (1990). The photochemical scheme of Buonsanto (1990) has been improved and now gives results similar to the more comprehensive scheme of (Solomon et al., 1988; Solomon and Abreu, 1989; S. C. Solomon and R. G. Roble, Simulation of the global thermospheric airglow, 1, Methodology, submitted to Journal of Geophysical Research, 1992), provided that the ratios of photoelectron impact ionization to photoionization (pe/pi) given by this latter model are included. The pe/pi ratios calculated by this model and by the models of Lilensten et al. (1989) and Richards and Torr (1988) differ significantly, and work is needed to resolve these differences. In general, the photochemical model results underestimate the data, especially in winter. This result agrees with that of the earlier paper by Buonsanto and could be resolved by decreasing MSIS-86 N_2 and O_2 densities in winter if additional ions were produced in the *E* region either by photoionization or by photoelectron impact ionization. The photoionization and photoabsorption cross sections of Conway (1988) give results in somewhat better agreement with observations than the cross sections of Torr et al. (1979). For the zenith angles considered (daytime conditions), the Chapman function method for calculating photoabsorption gives results in satisfactory agreement with a more rigorous calculation method using a formula from Rees (1989).

1. INTRODUCTION

Knowledge of the solar extreme ultraviolet (EUV) spectrum is of great importance for aeronomical modeling. The electron density (N_e) in the daytime *E-F1* region of the ionosphere is particularly sensitive to the EUV spectrum because of the approximate photochemical equilibrium which results at this region of maximum production by photoionization and electron impact ionization. None of the solar EUV radiation reaches the Earth's surface, so we have to rely on empirical models of the EUV fluxes, which are based on the limited data available from satellites and rockets. In this paper, we use different EUV flux models as input to two different photochemical schemes in order to calculate electron density profiles at Millstone Hill, Massachusetts (42.6°N, 288.5°E), on four different days when incoherent scatter radar N_e profiles are available. This procedure allows us to assess the sensitivity of the calculated profiles to the differences between the various flux models. Comparison of photochemical model results with observations provides a test of our current level of understanding, not only of the EUV spectrum, but also of photoionization and photoabsorption cross sections, reaction rates, secondary ionization by photoelectron impact, and neutral composition and temperature.

Since the early 1970s, several empirical solar EUV irradiance models have been developed for aeronomical applications. One early model was developed by *Donnelly and Pope* [1973] which tabulated measured EUV full-disk emissions for moderate solar activity. *Hinteregger et al.* [1981] developed the first proxy model based upon the Atmosphere Explorer E (AE-E) data set. A substantial contribution of this work was the development of the cycle 21 solar minimum reference spectrum called SC#21REFW. The Hinteregger et al. work described an EUV two-class (chromospheric and coronal) model which extended beyond the AE-E mission using a two variable (10.7-cm radio flux ($F10.7$) and the 81 day mean of $F10.7$) association formula. This work was later designated SERF1 by the Solar Electromagnetic Radiation Flux Study (SERFS). Following the release of SERF1, *Nusinov* [1984] developed a two-component model of full-disk solar EUV irradiance variation based upon

[1]Now at Jet Propulsion Laboratory, Pasadena, California.

Paper number 92JA00792.
0148-0227/92/92JA-00792$05.00

nonlinear regression formulas between $F10.7$ and the AE-E EUV fluxes. A further modeling effort by *Tobiska* [1988] developed a two-index EUV flux model using the Hinteregger et al. EUV class model concept while *Tobiska and Barth* [1990] improved the model by replacing a 1–8 Å X ray index with $F10.7$ daily values. This fourth empirical model was subsequently designated SERF2 [*Tobiska and Barth*, 1990; R. F. Donnelly, private communication, 1989].

SERF1 and SERF2 were compared by *Lean* [1990] over time scales of the 27-day solar rotation and the 11-year solar cycle. Significant differences were found between the models and between each model and the data sets upon which each was based. The differences appeared in the estimation of absolute intensities, the magnitude of peak-to-valley variation of irradiance due to solar rotation, and the maximum to minimum flux ratios over the 11-year solar cycle. The conclusion from this comparison indicated that neither models nor measurements yet provided a consistent picture of long-term variability in the EUV portion of the Sun's spectrum.

Following the comparisons of *Lean* [1990], another solar EUV flux model was developed [*Tobiska*, 1991] using a multiple linear regression technique. It represented an advance over the SERF1 and SERF2 models in proxy use, in modeling technique, in consistency between model and data, and in breadth of EUV data sets utilized in the correlations. In the present work, we use both SERF1 and the *Tobiska* [1991] model. The latter will be described more fully in section 4 below.

This paper follows on an earlier study [*Buonsanto*, 1990], in which a photochemical model was documented, and results compared with incoherent scatter data, ionosonde data, and ion composition models over a solar cycle. The conclusion of the earlier work was that increases of 25–30% in EUV fluxes above those based on the AE-E data, combined with decreases in MSIS-86 model densities input to the photochemical model were needed to obtain the best agreement with the N_e data and ion composition models. The decreases needed in the MSIS densities averaged 25%, with larger decreases needed in winter, and smaller or no decreases in summer. The photochemical model described by *Buonsanto* [1990] has been significantly improved as part of the present study, and the revisions to this model are described in section 2 below. In this study we also employ the photochemical and airglow/aurora model of [*Solomon et al.*, 1988; *Solomon and Abreu*, 1989; S. C. Solomon and R. G. Roble, Simulation of the global thermospheric airglow, 1, Methodology, submitted to *Journal of Geophysical Research*, 1992], hereinafter referred to as the Solomon model. This model is described in section 3.

2. Revisions to *Buonsanto* [1990] Model

The model described by *Buonsanto* [1990] was intended to include all photochemical reactions believed to be important in the region between 110 and 180 km in altitude. Photochemical equilibrium densities were calculated for $O^+(^4S)$, $O^+(^2D)$, N_2^+, O_2^+, and NO^+. The EUV fluxes in 37 wavelength bands were obtained by linear interpolation using $F10.7$ between the reference spectra for solar minimum (SC#21REFW) and solar maximum (F79050N) as published by *Torr and Torr* [1985]. The photoionization and photoabsorption cross sections in the same 37 wavelength bands were obtained from *Torr et al.* [1979]. At each wavelength, the photoabsorption was determined by the optical depth formula:

$$\tau = \Sigma\{\sigma_n^{(a)}[n]H_n\mathrm{Ch}(x_n,\chi)\} \quad (1)$$

where the summation is carried out over the neutral species (n) present (assumed to be O, N_2 and O_2), $\sigma_n^{(a)}$ is the photoabsorption cross section, $[n]$ is the concentration, and $H_n = kT_n/m_ng$ is the scale height of each neutral species, $\mathrm{Ch}(x_n,\chi)$ is the Chapman function, $x_n = (R_E + h)/H_n$, R_E is the Earth's radius, h is height, and χ is solar zenith angle. The rate of ionization by photoelectron impact was calculated using analytical expressions provided by *Lilensten et al.* [1989]. These expressions give the ratio of photoelectron impact ionization to photoionization (which we hereinafter refer to as pe/pi) in terms of solar zenith angle, latitude, and solar activity. However, they do not distinguish between neutral species, as we discuss further below. The MSIS-86 model [*Hedin*, 1987] provided the neutral densities and temperatures needed by the Buonsanto photochemistry. However, neutral nitric oxide (NO) is not included in MSIS-86, so simple [NO] models were constructed for Millstone Hill based on works by *Gérard et al.* [1984], *Stewart and Cravens* [1978], *Cravens et al.* [1985], and *Gérard and Noël* [1986].

We now describe the improvements made to the *Buonsanto* [1990] model, which we have implemented in the present study. Hereinafter we refer to this model with the improvements documented in this section as the revised Buonsanto model. Table 1 gives the ion-neutral and ion recombination reactions included in the revised model. The most significant change in the model is the inclusion of $O^+(^2P)$ chemistry, which has the effect of increasing the electron production rate. All the other changes in reaction rates or new reactions listed in Table 1 have a minor effect on the calculated ion and electron densities. They are listed so that the reader will have a fairly complete description of the revised model. The $N_2^+ + O_2$ reaction previously was included as a source of O_2^+. Now, for completeness, it is included as a sink for N_2^+ as well.

Some additional production is obtained in the revised model by inclusion of the $O^+(^4P)$ and $O^+(^2P^*)$ states (not shown in Table 1). Ions in the $O^+(^4P)$ state are assumed to decay promptly to $O^+(^4S)$, while $O^+(^2P^*)$ ions decay to either $O^+(^2D)$ or $O^+(^2P)$ with a branching ratio of 2.6:1 for $O^+(^2D)$:$O^+(^2P)$ [*Kirby et al.*, 1979].

In previous work, the photoabsorption rate was calculated using an analytic approximation [*Titheridge*, 1988] to the Chapman function (equation (1)), with the wavelength-dependent optical depth at each height depending on the scale heights of the neutral species at the given height. This method does not account for the changing scale heights in the overlying atmosphere. In the revised Buonsanto model a rigorous calculation of optical depth is carried out by integrating through the atmosphere using the MSIS-86 model and a formula provided by *Rees* [1989].

The revised Buonsanto model has three options for specifying pe/pi. These are the *Lilensten et al.* [1989] model used previously, the *Richards and Torr* [1988] model, and the Solomon model. In the previous work, pe/pi obtained from the

TABLE 1. Reactions Included in the Revised Buonsanto and Solomon Models

Reaction	Rate Coefficient (m^3s^{-1})	Reference
	Revised Buonsanto Model	
$O^+(^4S) + N_2 \rightarrow NO^+ + N$	$k_1 = 1.533\times10^{-18} - 5.92\times10^{-19}(T_f/300) + 8.6\times10^{-20}(T_f/300)^2$	1
$O^+(^4S) + O_2 \rightarrow O + O_2^+$	$k_2 = 1.25\times10^{-23}T_f^2 - 3.7\times10^{-20}T_f + 3.1\times10^{-17}$	2
$O^+(^2D) + N_2 \rightarrow O + N_2^+$	$k_3 = 8\times10^{-16}$	3
$O^+(^2D) + O_2 \rightarrow O + O_2^+$	$k_4 = 7\times10^{-16}$	3
$O^+(^2P) + O \rightarrow O^+(^4S) + O$	$k_5 = 5.2\times10^{-17}$	4
$O^+(^2P) + N_2 \rightarrow O + N_2^+$	$k_6 = 4.8\times10^{-16}$	4
$N_2^+ + O \rightarrow N_2 + O^+(^4S)$	$k_{7a} = 9.8\times10^{-18}(300/T_i)^{0.23}$	5
$N_2^+ + O \rightarrow N + NO^+$	$k_{7b} = 1.4\times10^{-16}(300/T_i)^{0.44} - k_{7a}$	5
$N_2^+ + O_2 \rightarrow N_2 + O_2^+$	$k_8 = 5\times10^{-17}(300/T)$	6
$O_2^+ + NO \rightarrow O_2 + NO^+$	$k_9 = 4.5\times10^{-16}$	6
$O_2^+ + N \rightarrow O + NO^+$	$k_{10} = 1.2\times10^{-16}$	7
$O_2^+ + e \rightarrow O + O$	$\alpha_1 = 2\times10^{-13}(300/T_e)^{0.7}$ $(T_e < 1200$ K)	8
	$\alpha_1 = 1.6\times10^{-13}(300/T_e)^{0.55}$ $(T_e \geq 1200$ K)	9
$NO^+ + e \rightarrow N + O$	$\alpha_2 = 4.3\times10^{-13}(300/T_e)$	10
	Solomon Model	
$O^+(^4S) + N_2 \rightarrow NO^+ + N$	$k_1 = 1.533\times10^{-18} - 5.92\times10^{-19}(T_f/300) + 8.6\times10^{-20}(T_f/300)^2$ $(T_f < 1700$ K)	
	$k_1 = 2.73\times10^{-18} - 1.155\times10^{-18}(T_f/300) + 1.483\times10^{-19}(T_f/300)^2$ $(T_f > 1700$ K)	1
$O^+(^4S) + O_2 \rightarrow O + O_2^+$	$k_2 = 2.82\times10^{-17} - 7.74\times10^{-18}(T_f/300) + 1.073\times10^{-18}(T_f/300)^2$ $- 5.17\times10^{-20}(T_f/300)^3 + 9.65\times10^{-22}(T_f/300)^4$	1
$O^+(^4S) + N(^2D) \rightarrow O + N^+$	$k_{11} = 1.3\times10^{-16}$	11
$O^+(^2D) + N_2 \rightarrow O + N_2^+$	$k_3 = 8\times10^{-16}$	3
$O^+(^2D) + O_2 \rightarrow O + O_2^+$	$k_4 = 7\times10^{-16}$	3
$O^+(^2D) + e \rightarrow O^+(^4S) + e$	$k_{12} = 6.6\times10^{-14}(300/T_e)^{0.5}$	12
$O^+(^2D) + O \rightarrow O^+(^4S) + O$	$k_{13} = 1\times10^{-17}$	13
$O^+(^2P) + N_2 \rightarrow O + N_2^+$	$k_6 = 4.8\times10^{-16}$	4
$O^+(^2P) + O_2 \rightarrow O + O_2^+$	$k_{14} = 4.8\times10^{-16}$	14
$O^+(^2P) + e \rightarrow O^+(^2D) + e$	$k_{15} = 1.7\times10^{-13}(300/T_e)^{0.5}$	12
$O^+(^2P) + O \rightarrow O^+(^4S) + O$	$k_5 = 5.2\times10^{-17}$	4
$N_2^+ + O \rightarrow N_2 + O^+(^4S)$	$k_{7a} = 2\times10^{-17}$	15
$N_2^+ + O \rightarrow N + NO^+$	$k_{7b} = 1.4\times10^{-16}(300/T_f)^{0.44}$	5
$N_2^+ + O_2 \rightarrow N_2 + O_2^+$	$k_8 = 5\times10^{-17}(300/T_f)^{0.8}$	16
$N_2^+ + e \rightarrow N + N$	$\alpha_3 = 1.8\times10^{-13}(300/T_e)^{0.39}$	17
$O_2^+ + NO \rightarrow O_2 + NO^+$	$k_9 = 4.4\times10^{-16}$	6
$O_2^+ + N \rightarrow O + NO^+$	$k_{10} = 1.2\times10^{-16}$	7
$O_2^+ + e \rightarrow O + O$	$\alpha_1 = 1.95\times10^{-13}(300/T_e)^{0.7}$ $(T_e < 1200$ K)	8,17,18
	$\alpha_1 = 1.6\times10^{-13}(300/T_e)^{0.55}$ $(T_e \geq 1200$ K)	9,17
$NO^+ + e \rightarrow N + O$	$\alpha_2 = 4.0\times10^{-13}(300/T_e)^{0.9}$	8,18
$N^+ + O_2 \rightarrow NO^+ + O$	$k_{16} = 2.6\times10^{-16}$	19
$N^+ + O_2 \rightarrow N + O_2^+$	$k_{17} = 3.1\times10^{-16}$	19
$N^+ + O \rightarrow N + O^+$	$k_{18} = 1\times10^{-18}$	20

Notes: $T_f = (m_iT_n + m_nT_i)/(m_n + m_i)$. (1) *St. Maurice and Torr* [1978]. (2) *Torr et al.* [1988]. (3) *Johnsen and Biondi* [1980]. (4) *Rusch et al.* [1977]. (5) *McFarland et al.* [1974]. (6) *Lindinger et al.* [1974]. (7) *Fehsenfeld* [1977]. (8) *Walls and Dunn* [1974]. (9) *Torr et al.* [1976]. (10) *Torr and Torr* [1979]. (11) *Bates* [1989]. (12) *Henry et al.* [1969]. (13) *Torr and Torr* [1980]. (14) *Link* [1982]. (15) *Knutsen et al.* [1988]. (16) *McFarland et al.* [1973]. (17) *Mehr and Biondi* [1969]. (18) *Alge et al.* [1983]. (19) *Langford et al.* [1985]. (20) *Torr* [1985].

formulation of Lilensten et al. was applied uniformly to all photoionization rates. In fact, the Lilensten et al. pe/pi formulation does not distinguish between species. However, for all three pe/pi model options we now apportion the atomic oxygen ions produced in the $O^+(^4S)$, $O^+(^2D)$, and $O^+(^2P)$ states in the ratios 0.56, 0.24, and 0.20 respectively, based on the work of *Richards and Torr* [1988]. This produces a little more $O^+(^4S)$ than in previous work.

A new neutral nitric oxide (NO) model for Millstone Hill is used. This is constructed from the tables of [NO] versus altitude and geomagnetic latitude provided by *Barth* [1990], which summarize data obtained from the polar-orbiting Solar

Mesosphere Explorer (SME) satellite for the period January 1982 to August 1986. The new model separates solar cycle, magnetic activity, and seasonal effects. As in earlier work, the diurnal variation of [NO] is based on the work of *Stewart and Cravens* [1978].

3. Description of Solomon Model

The Solomon model is a steady state photochemical model that employs detailed calculations of photoionization and photoelectron processes. Photoionization rates are calculated for each wavelength band in a manner similar to that described in section 2, except that excited and dissociated ion state production rates are calculated separately for the molecular ions as well as for atomic oxygen. The cross-section compilation of *Conway* [1988] was employed. These values differ from the earlier *Kirby et al.* [1979] compilation, upon which the *Torr et al.* [1979] band-averaged cross sections were based, primarily in that the atomic oxygen ionization cross section is reduced at the shorter wavelengths, following the measurements of *Samson and Pareek* [1985]. The cross sections were averaged for each wavelength band, weighted by the SC#21REFW solar minimum spectrum in that band. The solar flux may be specified using either the two-class contrast ratio, F10.7-association method [*Hinteregger*, 1981], linear interpolation between the SC#21REFW and F79050N spectra (as above), the *Tobiska* [1991] model (see below), or measured spectra. The solar spectrum extended from 18–1050 Å for all of the model runs shown below.

Photoelectron fluxes are computed using the two-stream method [*Banks and Nagy*, 1970; *Nagy and Banks*, 1970]. The photoelectron energy grid is extended to 700 eV so that the effects of photoionization down to a wavelength of 18 Å are included. Further details may be found in the works by *Solomon et al.* [1988] and *Solomon and Abreu* [1989]. The only important revision to the photoelectron calculations since these papers is a downward revision in some cross sections for excitation of ultraviolet transitions of atomic oxygen by photoelectron impact, resulting in approximate agreement with the total excitation cross section used by *Richards and Torr* [1988]. The cross sections employed for N_2 and O_2 are still significantly higher than those of Richards and Torr for energies greater than 20 eV, due to the inclusion of larger dissociation cross sections.

The electron density is calculated using the quartic equation solution of *Roble and Ridley* [1987]. The method is extended to include excited atomic oxygen ion states and the reaction of N_2^+ with O_2 to produce O_2^+. Chemical rate coefficients for ion-neutral and ion recombination reactions are listed in Table 1. They are similar to the revised Buonsanto model but also include some minor ion reactions that are only important at higher altitudes than examined in this work. The most significant difference between the ion chemistry in the two models is the different treatment of the reaction $O^+ + O_2 \rightarrow O_2^+ + O$. The Solomon model currently employs the formulation of *St. Maurice and Torr* [1978], while the Buonsanto model uses that of *Torr et al.* [1988], which is a fit to the measurements of *Chen et al.* [1978] in the 300–700 K range. The different rates for this reaction in the two models has a small effect on our calculated electron densities in the *F1* region, but hardly any effect in the *E* region, where the loss of electrons is controlled by dissociative recombination with NO^+ and O_2^+. Reasonable agreement has been obtained among several measurements of these dissociative recombination reactions [*Mehr and Biondi*, 1969; *Walls and Dunn*, 1974; *Alge et al.*, 1983; *Dulaney et al.*, 1987; *Davidson and Hobson*, 1987], and the rates used in the two models are very close. As in the Buonsanto model, the MSIS-86 neutral atmosphere model and NO densities from *Barth* [1990] are employed.

4. Empirical Solar EUV Irradiance Model of *Tobiska* [1991]

The solar EUV model of *Tobiska* [1991] was constructed using a multiple linear regression technique. The advantage of this type of algorithm is that many independent data sets, each appropriately weighted, may be used to determine correlations and model coefficients. With several independent proxy terms used for each of the chromospheric and coronal regressions, the model is capable of including new proxies to extend the model backward or forward in time, is able to take advantage of higher correlations obtained with mean value data (such as 81-day mean values), and is able to produce EUV irradiances with one proxy (such as $F10.7$) or multiple proxies, depending upon the user's needs.

In general, a chromospheric or coronal emission intensity I at a wavelength λ may be modeled as a time-varying quantity at 1 AU as

$$I(\lambda,t) = a_0(\lambda)A(t)+a_1(\lambda)F_1(t)+a_2(\lambda)F_2(t)+\ldots+a_n(\lambda)F_n(t) \quad (2)$$

in units of photons $cm^{-2}s^{-1}$ with n independent (proxy) terms according to the multiple linear regression technique described by *Bevington* [1969]. The $a_i(\lambda)$ coefficients are derived in the multiple linear regression, and $F_n(t)$ are the independent proxy data sets. $A(t)$ is a time vector with each element set to unity. This irradiance relationship is based on the assumption that the proxies vary linearly with the emissions with which they are being correlated. The assumption generally holds true for emissions which are created at the same temperature levels in the solar atmosphere. Missing proxy data are substituted through an empirical relationship with another proxy for which data do exist on given dates.

In the model, there are presently four proxy data sets used. $F_1(t)$ and $F_2(t)$ are the two chromospheric proxies, where $F_1(t)$ is the Lyman α flux and $F_2(t)$ is the He I 10,830-Å equivalent width (EW) scaled to Lyman α. $F_3(t)$ and $F_4(t)$ are the two coronal proxies, where $F_3(t)$ is the daily $F10.7$, and $F_4(t)$ is the 81-day running mean of $F10.7$. The 39 wavelength intervals used in the model are identical to the 37 intervals described by *Torr and Torr* [1985] with the addition of two intervals (18–30 and 31–50 Å). The EUV model is available from the National Space Science Data Center (NSSDC) at Goddard Space Flight Center and from the World Data Center A (WDC-A) for Solar-Terrestrial Physics in Boulder.

Six satellite EUV data sets, including OSO 1 (28.4 and 30.4 nm) [*Neupert et al.*, 1964], OSO 3 (25.6, 28.4, and 30.4 nm) [*Chapman and Neupert*, 1974], OSO 4 (30.4 nm) [*Timothy and Timothy*, 1970], OSO 6 (30.4 and 58.4 nm) [*Woodgate et al.*,

1973], AEROS A (28.4, 30.4, and 58.4 nm) [*Schmidtke et al.*, 1977], and AE-E (14.0-105.0 nm) [*Hinteregger et al.*, 1981], were used in the development of the solar EUV model. Each data set was weighted for instrument uncertainty. These EUV data were combined with data from six rocket flights, also weighted, to obtain the irradiances at EUV wavelengths for correlation with the model proxies. The six rockets included three ionization cell or silicon photodiode instruments flown by the University of Southern California and described by *Carlson et al.* [1984], *Ogawa and Judge* [1986], and *Ogawa et al.* [1990], two spectrographs flown by the University of Colorado described by *Woods and Rottman* [1990] and T. N. Woods (private communication, 1991), and one spectrometer flown by the Air Force Geophysics Laboratory described by *Van Tassel et al.* [1981]. The model proxy data sets which are used to establish a correlation between either chromospheric or coronal irradiances or to extend the estimate of these irradiances outside the original EUV data time frames, include the Solar Mesosphere Explorer (SME) Lyman α described by *Barth et al.* [1990], the AE-E Lyman α described by *Hinteregger et al.* [1981], the OSO 4 Lyman α described by *Timothy and Timothy* [1970], the OSO 6 Lyman α described by *Woodgate et al.* [1973], the He I 10,830-Å equivalent width (EW) described by *Harvey* [1984], and the Ottawa $F10.7$ provided by the World Data Center A.

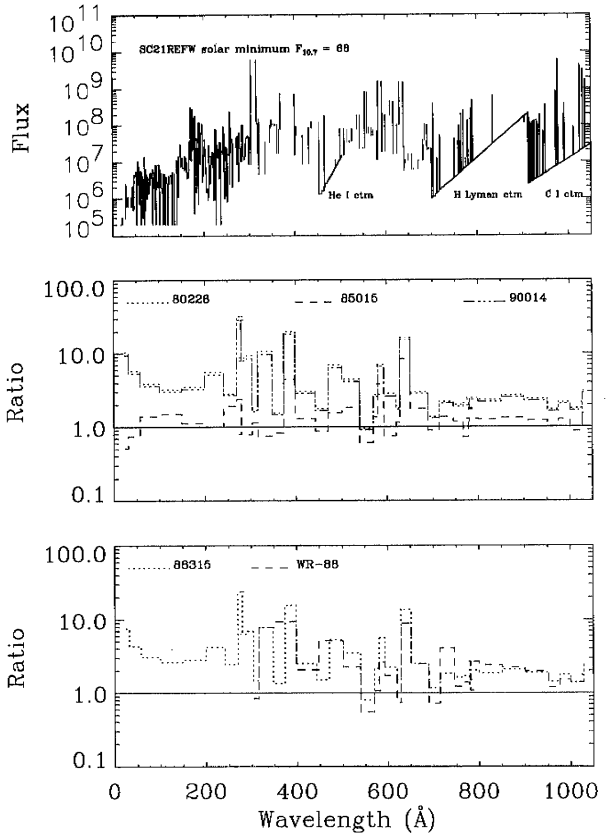

Fig. 1. The solar spectra for the *Tobiska* [1991] model compared to the SC#21REFW spectrum [*Hinteregger et al.*, 1981] in 39 wavelength intervals between 18 and 1050 Å. The top panel shows the high resolution reference spectrum for solar cycle 21 minimum when $F10.7$ = 68. The middle and bottom panels show the ratio of the Tobiska EUV model spectra to SC#21REFW where each model spectrum on a given date is denoted by a differently labeled line. Day 226 of 1980 is 80226, while WR-88 is the November 10, 1988, *Woods and Rottman* [1990] spectrum.

In Figure 1, the EUV model of *Tobiska* [1991] is compared with the SC#21REFW spectrum described by *Hinteregger et al.* [1981] for four different levels of solar activity and with the *Woods and Rottman* [1990] rocket flight spectrum of November 10, 1988 (day 88315). In the first panel, the spectrum is shown from 18 to 1050 Å where continua and line emissions are both observed. In the second and third panels, the ratio of the 39 wavelength group binned solar flux to the SC#21REFW spectrum is shown for 80226 ($F10.7$ = 193, high activity), for 85015 ($F10.7$ = 72, low activity), for 90014 ($F10.7$ = 166, moderate activity), and for 88315 ($F10.7$ = 148, moderate activity). All model EUV flux values, by date and throughout most of the spectrum, are higher than the reference spectrum, although the low solar activity case is generally comparable while discrete lines differ the most from the overall reference spectrum.

5. Description of the November 1988 Rocket Experiment

The solar EUV flux was measured on November 10, 1988 (day 88315), 1900 UT (local noon) at White Sands Missile Range by a spectrograph carried on a Black Brant IV sounding rocket, which obtained apogee of 237 km. The instrument and results are described by *Woods and Rottman* [1990]. Preflight and postflight calibrations indicated an average photometric uncertainty of 6%; inclusion of uncertainties due to atmospheric absorption resulted in estimated uncertainties from 6–23%, depending on wavelength. To utilize the measured fluxes in the photoionization calculations, individual line intensities are taken from their Table 1, and 50 Å "continuum" fluxes from their Table 2. Some minor lines included in Table 1 are not part of the standard *Torr and Torr* [1985] set and so are added to the corresponding 50 Å bin; conversely, a few weak lines in the Torr and Torr set not extracted from the rocket data are treated by using model values and subtracting that amount from the 50 Å bin. Thus the total measured flux is preserved with respect to each 50-Å interval. One correction is made to the measured spectrum: the He I line at 585 Å is increased by 70% (to 1.71 × 10^9 cm^{-2} s^{-1}) to account for the effect of instrument saturation (T. N. Woods, private communication, 1991). The spectrograph range was from 300 to 1100 Å. The Tobiska model for November 10, 1988, is used to extend the "measured" spectrum down to 18 Å in the model calculations which follow.

6. Electron Density Profiles From Incoherent Scatter Measurements

The Millstone Hill (42.6°N, 288.5°E) incoherent scatter profiles were obtained using a short (40 μs) pulse with 6 km altitude resolution. These profiles were calibrated using *foF2* from the local Digisonde, and temperature and Debye length corrections were applied using the best ion and electron temperature profiles that could be constructed from the available longer pulse measurements at the greater heights and

from the MSIS-86 model at the lower heights [*Buonsanto*, 1989, 1990]. Representative error bars are calculated at 120 km and 150 km using the method outlined by *Evans* [1969]. Since it is extremely difficult to simultaneously fit incoherent scatter spectra in the *E* and *F1* regions for temperatures and ion composition, a standard ion composition profile is assumed in the reduction of Millstone Hill data, which assumes 50% O^+ at 180 km. As done by *Buonsanto* [1990], we use ion composition profiles calculated by the revised Buonsantc model, together with factors given by *Waldteufel* [1971], to correct the observed incoherent scatter N_e, T_e, and T_i measurements. The revised temperatures are then input to the model and a new profile calculated. This procedure is repeated iteratively until convergence to final temperature and ion composition profiles.

7. Results and Discussion

Photoionization rates calculated using the Solomon model for five solar flux cases are shown in Figure 2 for November 10, 1988, at 1517 UT, to correspond to the time of the electron density measurement. Three different versions of the Hinteregger solar flux model are plotted: the two-class contrast ratio and linear interpolation methods as described above, and a third case in which the contrast ratio method is used but the flux shortward of 250 Å is multiplied by a factor of 2 as suggested by *Richards and Torr* [1984, 1988]. This adjustment obtains better agreement with photoelectron measurements and with broadband solar flux measurements [*Ogawa and Judge*, 1986] and also brings the Hinteregger model into closer agreement with the Tobiska model at the shorter wavelengths. Using linear interpolation on *F*10.7 produces a lower photoionization rate at all altitudes, because the 81-day average value of *F*10.7, an important input to the contrast ratio method, was 167, considerably higher than the daily value of 148. Photoionization rates using the Tobiska model and the Woods and Rottman measurement are also plotted. These have a lower photoionization rate in the 100–120 km region, because the longer wavelength fluxes, particularly H Lyman β at 1026 Å, are smaller.

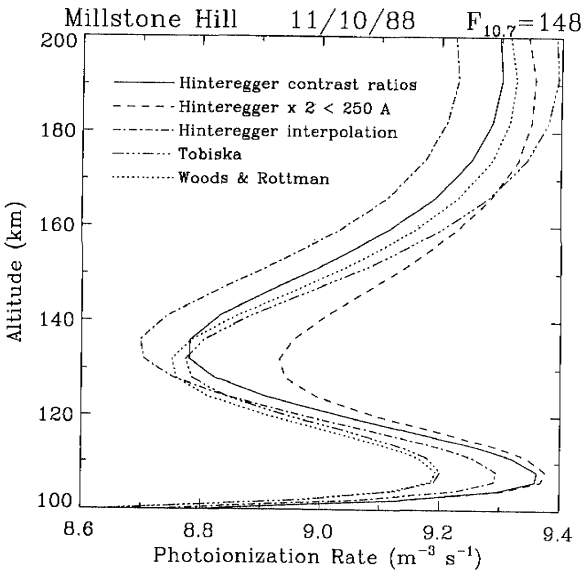

Fig. 2. Photoionization rates calculated using the Solomon model for five solar flux cases and 1517 UT on November 10, 1988, at Millstone Hill (log units).

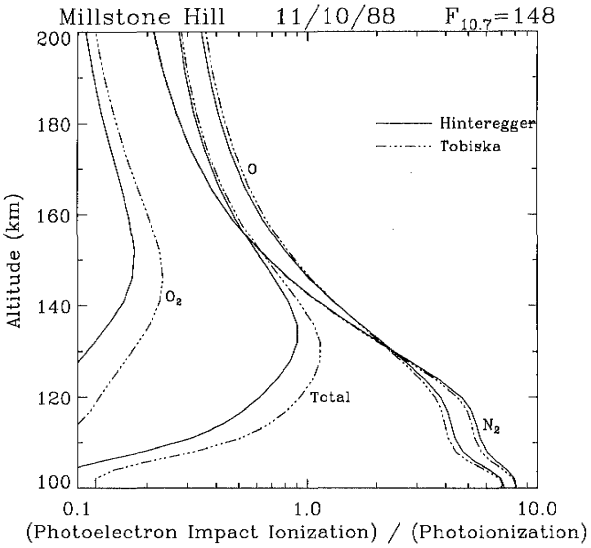

Fig. 3. Pe/pi ratios for O, N_2, and O_2 calculated by the Solomon model using two EUV flux models for 1517 UT on November 10, 1988, at Millstone Hill.

Ratios of photoelectron impact ionization to photoionization for two of these model calculations are plotted in Figure 3. These ratios are in effect enhancement factors to the direct photoionization rates and are weakly dependent upon the solar spectrum. Here the Hinteregger contrast ratio and Tobiska models are used. The total ratio reaches a peak in the *E-F1* valley region, where short-wave EUV photons and soft X rays deposit their energy, and declines in the *E* region, where ionization of O_2 by longer wavelength EUV dominates the photoionization rate profile.

Comparisons between observed Millstone Hill incoherent scatter N_e profiles and profiles calculated using the Solomon model are given for 1517 UT (1031 local mean time, or LMT) on November 10, 1988, in Figure 4, for 1813 UT (1327 LMT) on January 15, 1985, in Figure 5, for 1557 UT (1111 LMT) on January 14, 1990, in Figure 6, and for 1646 UT (1200 LMT) on August 13, 1980, in Figure 7. In each of the four figures, curve a shows N_e calculated from contrast ratio scaling using the Atmosphere Explorer two-class model and *F*10.7 association formula [*Hinteregger et al.*, 1981]; curve b shows N_e calculated as for curve a, except with the EUV fluxes at wavelengths less than 250 Å increased by a factor of 2; curve c shows N_e calculated using EUV fluxes interpolated linearly using *F*10.7 between the SC#21REFW and F79050N reference spectra, as done by *Buonsanto* [1990]; and curve d shows N_e calculated using EUV fluxes from the *Tobiska* [1991] model, as described in section 4 above. In Figure 4 only, curve e shows N_e calculated using EUV fluxes measured by the November 10, 1988, rocket experiment described by *Woods and Rottman* [1990].

For each of the four cases (Figures 4–7), the calculated profiles underestimate the observations at most heights. The *Tobiska* [1991] model fluxes are in best agreement with the rocket measurements shown in Figure 4. This is expected, since

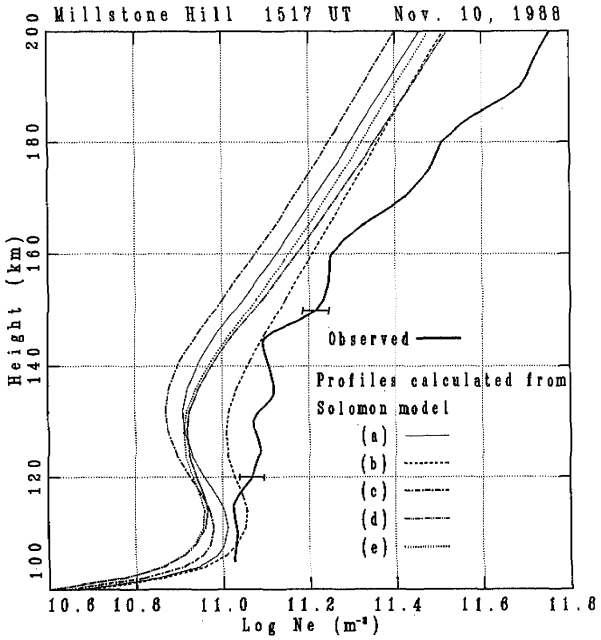

Fig. 4. Electron density profiles at Millstone Hill for 1517 UT (1031 LMT) on November 10, 1988. Heavy solid line: observed incoherent scatter profile. Key for EUV flux models used in profiles calculated with the Solomon photochemical model: (*a*) *Hinteregger et al.* [1981] model; (*b*) Hinteregger et al. model except that fluxes at wavelengths less than 250 Å have been doubled; (*c*) Linear interpolation using *F*10.7 between SC#21REFW and F79050N reference spectra; (*d*) *Tobiska* [1991] model; (*e*) rocket flight measurements [*Woods and Rottman*, 1990].

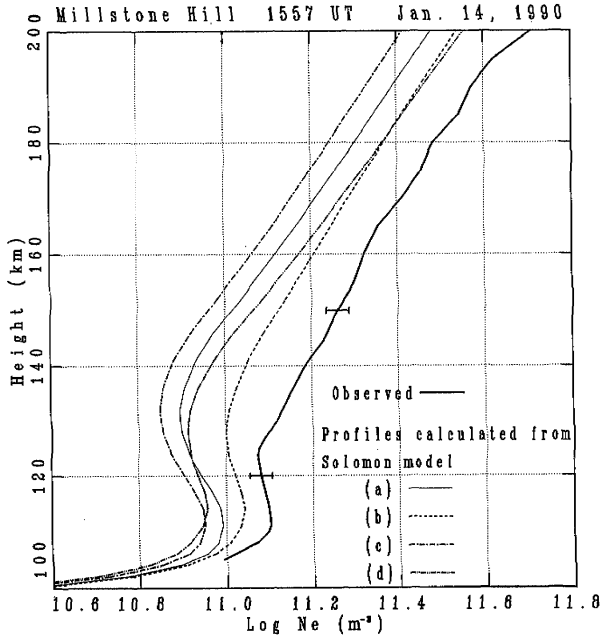

Fig. 6. Same as Figure 5, except for 1557 UT (1111 LMT) on January 14, 1990.

the rocket measurements are incorporated into the Tobiska model. Although the Tobiska model has generally more flux than the *Hinteregger et al.* [1981] model at short wavelengths, it has generally less at Lyman β (1025.7 Å). This is partially due to the low measurement of Lyman β by *Woods and Rottman* [1990] compared to both the AE-E data and a June 1989 rocket experiment (T. N. Woods, private communication, 1991). Lyman β radiation is important for photoionization of O_2 in the *E* region. Thus the Hinteregger et al. model gives a slightly higher *foE*, which is closer to the measurements. Since the incoherent scatter observations shown in Figure 4 were taken essentially simultaneously with the rocket measurements, the

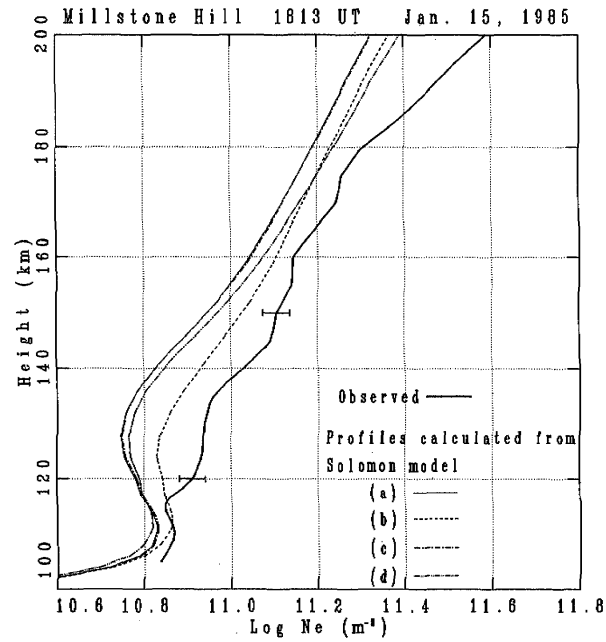

Fig. 5. Same as Figure 4, except for 1813 UT (1327 LMT) on January 15, 1985, and no rocket flight data available.

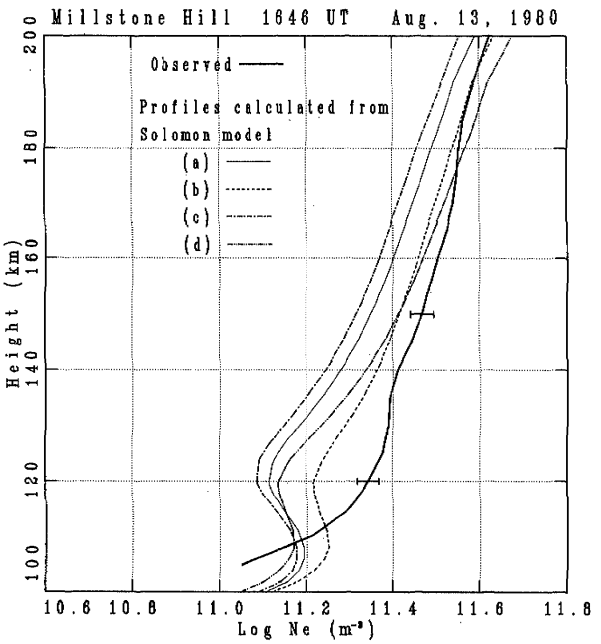

Fig. 7. Same as Figure 5, except for 1646 UT (1200 LMT) on August 13, 1980.

low value of Lyman β measured by the rocket experiment may be incorrect (low by perhaps 40%), as opposed to being correct but atypical for this stage of the solar cycle. Because the Tobiska model has generally greater fluxes than the Hinteregger et al. model at the short end of the spectrum, N_e calculated using the Tobiska fluxes are generally in better agreement with the observed profiles at the greater heights (the *E-F1* valley and above). Best agreement at the greater heights is obtained for the August, 13, 1980, case (Figure 7). This agrees with the conclusion of *Buonsanto* [1990] that calculated and observed profiles agreed best in summer. Overall best agreement with the data from all four cases is obtained using the Hinteregger et al. model with the fluxes at wavelengths below 250 Å increased by a factor of 2 (curves labeled b).

From our discussion above, it is clear that when any of the EUV flux models in current use, or even the observed fluxes on November 10, 1988, are input to the comprehensive photochemical scheme of Solomon, calculated N_e profiles generally underestimate the data. This result is consistent with the results of earlier work [*Buonsanto*, 1990], where it was shown that increases of 25–30% in EUV fluxes were needed to calculate N_e in agreement with the observations. The earlier work obtained EUV fluxes by linear interpolation using $F10.7$ between the SC#21REFW and F79050N reference spectra. We follow this same method to calculate the Solomon model profiles shown in Figures 4–7 by the curves labeled c.

Two independent photochemical schemes were used in the current work. We show in Figures 8–11 comparison of observed profiles with the results of calculations using both the Solomon photochemical model, and the revised Buonsanto model. The Solomon photochemical scheme is the more comprehensive of the two, however both models include all processes known to be important for the calculation of electron density profiles in *E* and *F1* regions. The most significant difference between the two models is that while the Solomon model explicitly calculates photoelectron fluxes and their effects,

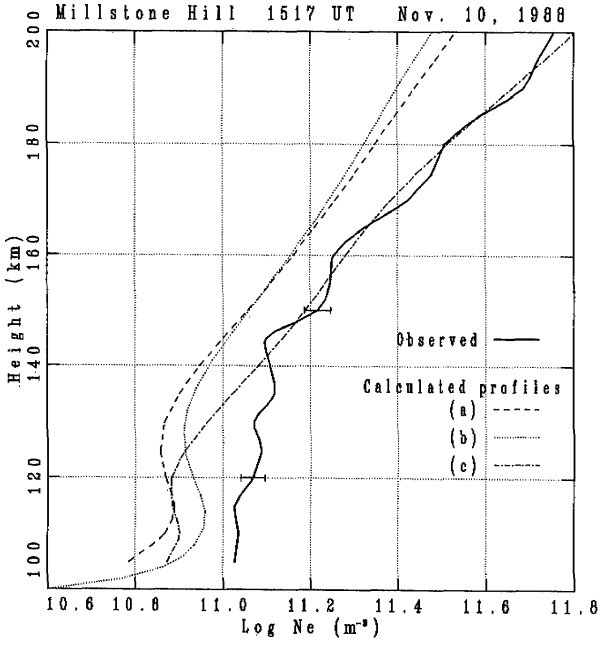

Fig. 8. Electron density profiles at Millstone Hill for 1517 UT (1031 LMT) on November 10, 1988. Heavy solid line: observed incoherent scatter profile. Key for calculated profiles: (*a*) revised Buonsanto photochemical model; (*b*) Solomon photochemical model; (*c*) revised Buonsanto photochemical model with MSIS-86 $[N_2]$ and $[O_2]$ multiplied by 0.5.

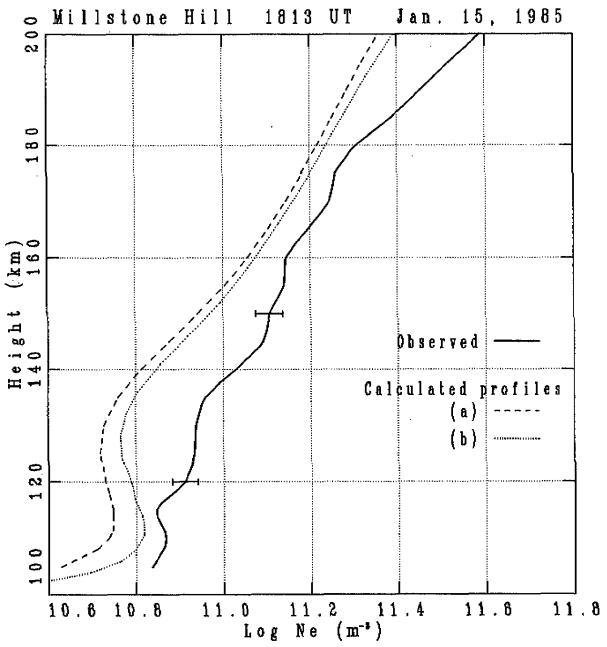

Fig. 9. Same as Figure 8, except for 1813 UT (1327 LMT) on January 15, 1985, and no curve c.

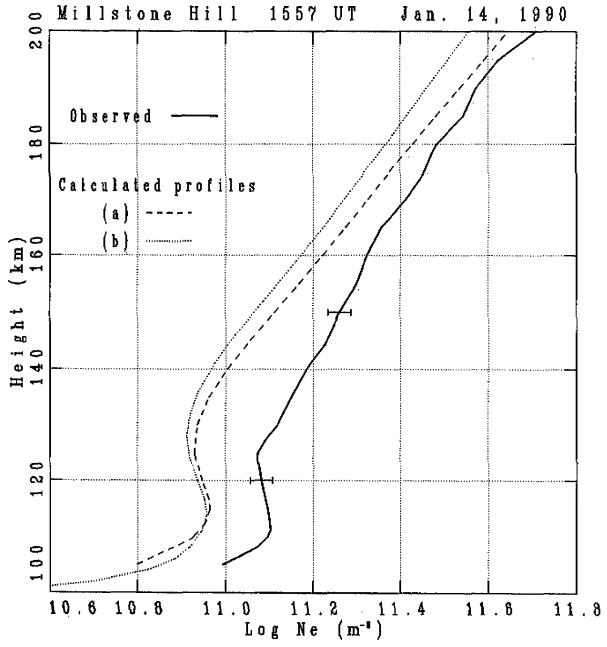

Fig. 10. Same as Figure 9, except for 1557 UT (1111 LMT) on January 14, 1990.

the most important for the work described here being photoelectron impact ionization, the revised Buonsanto model relies on pe/pi ratios obtained from other sources. As discussed above, three options for pe/pi in the revised Buonsanto model are available: the models of *Richards and Torr* [1988], *Lilensten et al.* [1989], and Solomon. For the comparisons in Figures 8–11, the Buonsanto model used the pe/pi ratios and cross sections from the Solomon model.

Figure 8 shows the comparison between the observations and the two photochemical models for November 10, 1988. The EUV fluxes used in the model calculations were obtained from the *Woods and Rottman* [1990] rocket measurements. Results from the two models underestimate the observations, with the differences between the two models being generally much less than the differences between either model and the observations. The revised Buonsanto model (curve a) agrees a little better with the observations above $\approx$ 150 km while the Solomon model (curve b) does a little better in E region. Curve c in Figure 8 shows results from the revised Buonsanto model when MSIS-86 $[N_2]$ and $[O_2]$ are decreased by a factor of 2. A good match with observations is obtained above 140 km because of the decrease in photoabsorption. However, there is little improvement in the E region, because the decreased photoabsorption is offset by a decreased photoionization. *Buonsanto* [1990] found that decreases in MSIS-86 $[N_2]$ and $[O_2]$ in winter had to be combined with increases in EUV fluxes to obtain model results in agreeement with observed N_e profiles. We could match the observations shown in Figure 8 if the 50% decrease in MSIS-86 $[N_2]$ and $[O_2]$ were combined with an enhancement in some process which results in greater ionization below 140 km. Examples of such processes are photoionization due to short wavelength radiation (< 200 Å), Lyman β and other long wavelength radiation, and photoelectron impact ionization, all of which maximize in this region. Figures 9–11 show comparisons for the other three days between the observed N_e profiles and the two photochemical models, where the EUV fluxes are obtained from the *Tobiska* [1991] model. These figures show that the revised Buonsanto model and the Solomon model generally give similar results. As discussed above, the profiles calculated by both models systematically underestimate the observed profiles for all cases except the summer one (Figure 11). This is consistent with the results of the earlier study [Buonsanto, 1990], which found better agreement between the model and the observations in summer.

The major discrepency between the model and observed profiles for the summer case (Figure 11) is the lack of an observed *E-F1* valley. While the valley is very clearly seen in the incoherent scatter measurements shown in Figure 10, the observed valleys in Figures 8 and 9 are not distinct at all and could even represent signatures of gravity waves or noise in the measurements. The 6 km altitude resolution of the incoherent scatter data would be more than adequate for observing an *E-F1* valley of the width predicted by the two models. Examination of many additional Millstone Hill N_e profiles reveals that the *E-F1* valley appears frequently, but not always, in the data. By contrast, it is a regular feature of the model results.

One source of uncertainty in the photochemical models is in the specification of photoelectron impact ionization. This is

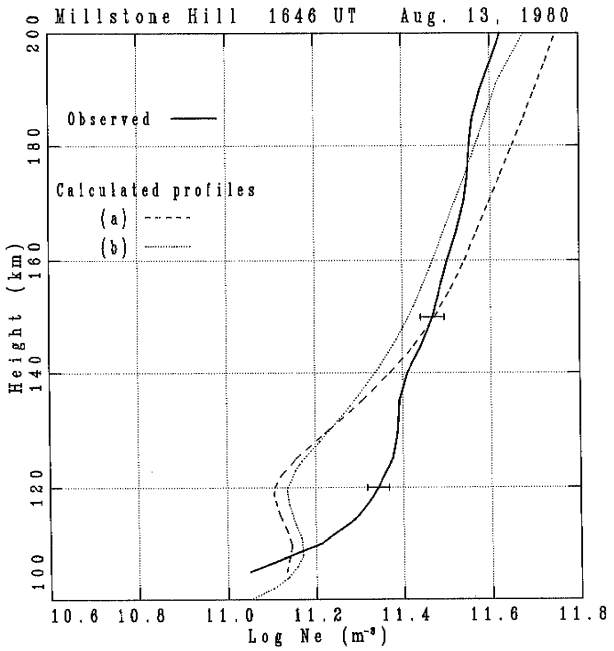

Fig. 11. Same as Figure 9, except for 1646 UT (1200 LMT) on August 13, 1980.

illustrated by Figure 12, where we plot a comparison of the observed N_e profile for November 10, 1988 with profiles calculated using the *Woods and Rottman* [1990] EUV fluxes for this day input to the revised Buonsanto model with the three different pe/pi options. Curve a shows results obtained using

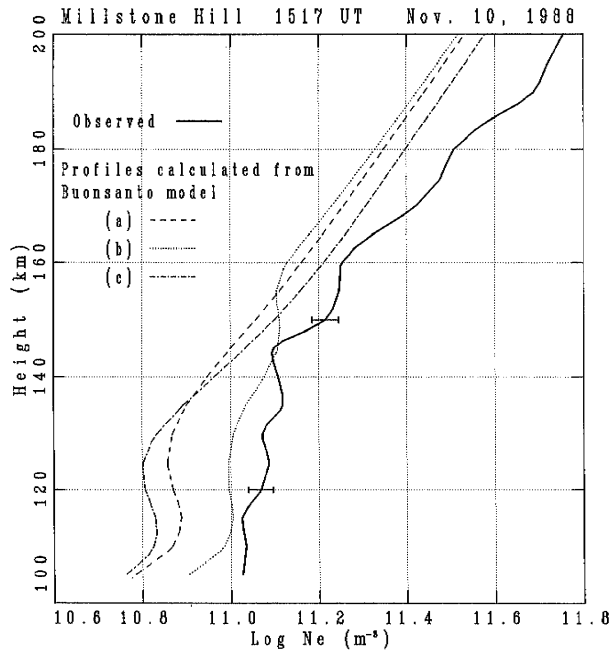

Fig. 12. Electron density profiles at Millstone Hill for 1517 UT (1031 LMT) on November 10, 1988. Heavy solid line: observed incoherent scatter profile. Key for pe/pi models used in profiles calculated with the revised Buonsanto photochemical model: (*a*) Solomon; (*b*) *Lilensten et al.* [1989]; (*c*) *Richards and Torr* [1988].

pe/pi from the Solomon model. This option was used for all other model calculations presented in this study, except for curves b and c in this figure. Curve b shows results obtained using the *Lilensten et al.* [1989] pe/pi model which was previously used by Buonsanto [1990]. Curve c shows results obtained using the pe/pi model of *Richards and Torr* [1988].

Comparison of the pe/pi profiles from the Solomon model shown in Figure 3 to those of Lilensten et al. and Richards and Torr reveals significant discrepancies between these three calculations. At high (*F* region) altitudes, the Solomon and Lilensten et al. calculations are in reasonable agreement (with respect to the total ratio, which is the quantity plotted by Lilensten et al.) but the Lilensten et al. pe/pi reaches a factor of almost 2 near 120 km, while the Solomon total ratio peaks at ~1 near 130 km. The Richards and Torr ratios, which are broken down by species, agree adequately with the Solomon ratios at this altitude but become considerably larger with increasing altitude, especially in the case of N_2. This is probably due to the larger electron impact excitation cross sections for N_2 and O_2 used by Solomon than by Richards and Torr, which has the effect of decreasing the photoelectron flux. The Richards and Torr calculation did not extend below 120 km, as their photoelectron spectrum was truncated at 100 eV. The Lilensten et al. calculation extended to 250 eV, while the Solomon model extends, in this instance, to 700 eV. The Lilensten et al. model gives N_e values in better agreement with the observations in the *E* region. However, an unrealistic kink in the profile is produced near 150 km, due to a rapid falloff of pe/pi above ~140 km.

Another source of uncertainty in the photochemical models is in the photoionization and photoabsorption cross sections. *Buonsanto* [1990] used the cross sections in 37 wavelength bins provided by *Torr et al.* [1979]. In this study we use the cross sections (in 39 wavelength bins) of the Solomon model, which are based on the compilation by *Conway* [1988]. In Figure 13 we plot a comparison of the observed profile for November 10, 1988, with calculated profiles obtained using the two different sets of cross sections. Again, the revised Buonsanto model was used, with the *Woods and Rottman* [1990] EUV fluxes for this day. The Conway cross sections result in more ionization in *E-F1* valley and up to nearly 200 km, in better agreement with the observations. This is because the reduced atomic oxygen cross section at short wavelengths allows more radiation to penetrate to the *E-F1* valley.

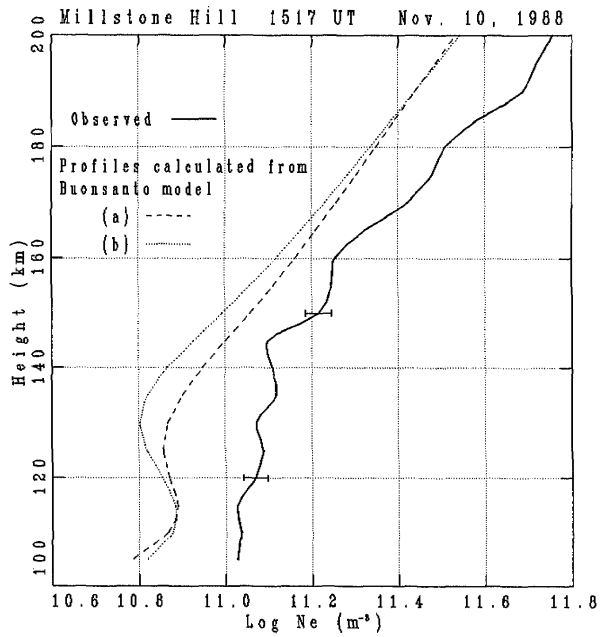

Fig. 13. Electron density profiles at Millstone Hill for 1517 UT (1031 LMT) on November 10, 1988. Heavy solid line: observed incoherent

An improvement of the revised *Buonsanto* model over the earlier version is the rigorous calculation of photoabsorption, using the formula of *Rees* [1989]. Comparison of results obtained using both the Chapman function method and the new, more rigorous method show that the Chapman function method does quite well for the solar zenith angles considered in the study (daytime conditions).

Conclusions

The *Tobiska* [1991] EUV flux model has generally more flux than the *Hinteregger et al.* [1981] model at short wavelengths. This results in larger calculated electron densities in the *E-F1* valley region and above, in better overall agreement with the observed N_e profiles. However,the Tobiska EUV flux model has generally less flux at Lyman β (1025.7 Å), compared to the Hinteregger et al. model. This is partially due to the relatively low flux measured at Lyman β by the November 10, 1988, rocket experiment [*Woods and Rottman*, 1990], as this data set is included in the Tobiska model. The result is that the Hinteregger et al. fluxes give a larger *foE*, in better agreement with observations, than the Tobiska fluxes do.

The *Hinteregger et al.* [1981] and *Tobiska* [1991] solar flux models, while good for first-order approximations to the solar irradiance for a given date, still both contain substantial uncertainty compared to measurements on any given date. This argues for a concerted effort to improve solar measurements and models in the next few years and demonstrates that uncertain solar irradiance continues to contribute significant uncertainty to ionospheric calculations.

The *Buonsanto* [1990] photochemical equilibrium model has been improved and the revised model is shown to give results similar to those of the more comprehensive Solomon model, when the Solomon pe/pi ratios are included. Of the four cases, three were in "winter". At these times the model results underestimated the data. For the summer case, better agreement was obtained, except for the absence of an observed *E-F1* region valley. While the valley appeared in all the model results, it is a more transient feature in the data. A decrease in $[N_2]$ and $[O_2]$ by a factor of 2 from the MSIS-86 model values for the November 1988 case gave excellent results at the greater heights, but did not improve the agreement significantly with the observed N_e profile in the *E* region. Additional *E* region ionization would be obtained if increased photoionizing fluxes at appropriate wavelengths or larger pe/pi ratios are used in this region. The pe/pi ratios in the models of *Richards and Torr* [1988], *Lilensten et al.* [1989], and *Solomon* differ significantly,

and work is needed to resolve these differences. Cross sections in the Solomon model, based on the compilation by Conway [1988], give a little more E region ionization than the cross sections of *Torr et al.* [1979], in better agreement with observations. The Chapman function method for calculating photoabsorption is shown to give satisfactory results for daytime conditions, when compared with the more rigorous calculation method described by *Rees* [1989].

Acknowledgments. The authors thank T. N. Woods and G. J. Rottman, University of Colorado Laboratory for Atmospheric and Space Physics, for providing and discussing their solar measurements. R. Link of Computational Physics, Inc. graciously provided assistance in evaluating the species cross sections used in this study. The MSIS-86 Thermospheric Model was kindly provided by A. E. Hedin of the Goddard Space Flight Center, Greenbelt, Maryland. Millstone Hill data were acquired and analyzed under the support of National Science Foundation Cooperative Agreements ATM-8808137 and ATM-9102445 to the Massachusetts Institute of Technology. Work by S. C. Solomon was supported by NSF grant ATM-900111 and NASA grant NAGW-2116 to the University of Colorado. Work by W. K. Tobiska was supported by National Science Foundation grant NSF FD89-00145 and by California Space Institute (Calspace) grant CALSPACE CS-35-90.

The Editor thanks A. F. Nagy and another referee for their assistance in evaluating this paper.

REFERENCES

Alge, E., N. G. Adams, and D. Smith, Measurements of the dissociative recombination coefficients of O_2^+, NO^+, and NH_4^+ in the temperature range 200–600 K, *J. Phys. B, 16*, 1433–1444, 1983.

Banks, P. M., and A. F. Nagy, Concerning the influence of elastic scattering upon photoelectron transport and escape, *J. Geophys. Res.*, *75*, 1902–1910, 1970.

Barth, C. A., Reference models for thermospheric NO, *Adv. Space Res., 10*(6), 103–115, 1990.

Barth, C. A., W. K. Tobiska, G. J. Rottman, and O. R. White, Comparison of 10.7 cm radio flux with SME solar Lyman alpha flux, *Geophys. Res. Lett., 17*, 571–574, 1990.

Bates, D. R., Theoretical considerations regarding some inelastic atomic collision processes of interest in aeronomy: Deactivation and charge transfer, *Planet. Space Sci., 37*, 363–368, 1989.

Bevington, P. R., *Data Reduction and Error Analysis for the Physical Sciences*, 336 pp., McGraw Hill, New York, 1969.

Buonsanto, M. J., Comparison of incoherent scatter observations of electron density, and electron and ion temperature at Millstone Hill with the International Reference Ionosphere, *J. Atmos. Terr. Phys., 51*, 441–468, 1989.

Buonsanto, M. J., A study of the daytime *E-F1* region ionosphere at mid-latitudes, *J. Geophys. Res.*, *95*, 7735–7747, 1990.

Carlson, R. W., H. S. Ogawa, E. Phillips, and D. L. Judge, Absolute measurements of the extreme UV solar flux, *Appl. Opt., 23*, 2327–2332, 1984.

Chapman, R. D., and W. M. Neupert, Slowly varying component of extreme ultraviolet solar radiation and its relation to solar radio radiation, *J. Geophys. Res., 79*, 4138–4148, 1974.

Chen, A., R. Johnsen, and M. A. Biondi, Measurements of the $O^+ + N_2$ and $O^+ + O_2$ reaction rates from 300 to 900 K, *J. Chem. Phys., 69*, 2688–2691, 1978.

Conway, R. R., Photoabsorption and photoionization cross sections of O, O_2, and N_2 for photoelectron production calculations: A compilation of recent laboratory measurements, *NRL Mem. Rep. 6155*, Nav. Res. Lab., Washington, D. C., 1988.

Cravens, T. E., J.-C. Gérard, M. LeCompte, A. I. Stewart, and D. W. Rusch, The global distribution of nitric oxide in the thermosphere as determined by the Atmosphere Explorer D satellite, *J. Geophys. Res., 90*, 9862–9870, 1985.

Davidson, D., and R. Hobson, The shock tube determination of the dissociative recombination rate of NO^+, *J. Phys. B., 20*, 5753–5756, 1987.

Donnelly, R. F., and J. H. Pope, The 1–3000 Å solar flux for a moderate level of solar activity for use in modeling the ionosphere and upper atmosphere, *NOAA Tech. Rep. ERL 276-SEL 25*, Natl. Oceanic and Atmos. Admin., Boulder, Colo., 1973.

Dulaney, J., M. Biondi, and R. Johnsen, Electron temperature dependence of the recombination of electrons with NO^+ ions, *Phys. Rev. A. Gen. Phys., 36*, 1342–1350, 1987.

Evans, J. V., Theory and practice of ionosphere study by Thomson scatter radar, *Proc. IEEE, 57*, 496–530, 1969.

Fehsenfeld, F. C., The reaction of O_2^+ with atomic nitrogen and $NO^+ \cdot H_2O$ and NO_2^+ with atomic oxygen, *Planet. Space Sci., 25*, 195–196, 1977.

Gérard, J. C., and C. E. Noël, AE-D measurements of the NO geomagnetic latitudinal distribution and contamination by $N^+(^5S)$ emission, *J. Geophys. Res., 91*, 10,136–10,140, 1986.

Gérard, J. C., R. G. Roble, D. W. Rusch, and A. I. Stewart, The global distribution of thermospheric odd nitrogen for solstice conditions during solar cycle minimum, *J. Geophys. Res., 89*, 1725–1738, 1984.

Harvey, J., Helium 10830 Å irradiance: 1975-1983, Solar Irradiance Variations on Active Region Time Scales, edited by B. LaBonte, G. Chapman, H. Hudson, and R. Wilson, *NASA Conf. Publ., CP-2310*, 197–211, 1984.

Hedin, A. E., MSIS-86 thermospheric model, *J. Geophys. Res., 92*, 4649–4662, 1987.

Henry, R. J. W., P. G. Burke, and A. L. Sinfailam, Scattering of electrons by C, N, O, N^+, O^+, and O^{++}, *Phys. Rev., 178*, 218–224, 1969.

Hinteregger, H. E., K. Fukui, and B. R. Gilson, Observational, reference and model data on solar EUV, from measurements on AE-E, *Geophys. Res. Lett., 8*, 1147–1150, 1981.

Johnsen, R., and M. A. Biondi, Laboratory measurements of the $O^+(^2D) + N_2$ and $O^+(^2D) + O_2$ reaction rate coefficients and their ionospheric implications, *Geophys. Res. Lett., 7*, 401–403, 1980.

Kirby, K., E. R. Constantinides, S. Babeu, M. Oppenheimer, and G. A. Victor, Photoionization and photoabsorption cross sections of thermospheric species: He, O, N_2, and O_2, *At. Data Nucl. Data Tables, 23*, 63–81, 1979.

Knutsen, K., V. Bierbaum, and S. Leone, Remeasurement of the rate constant and branching ratio for the $N_2^+ + O$ reaction, *Planet. Space Sci., 36*, 307–310, 1988.

Langford, A. O., V. M. Bierbaum, and S. R. Leone, Auroral implications of recent measurement of $O(^1S)$ and $O(^1D)$ formation in the reaction of N^+ with O_2, *Planet. Space Sci., 33*, 1225–1228, 1985.

Lean, J., A comparison of models of the Sun's extreme ultraviolet irradiance variations, *J. Geophys. Res., 95*, 11,933–11,944, 1990.

Lilensten, J., W. Kofman, J. Wisemberg, E. S. Oran, and C. R. Devore, Ionization efficiency due to primary and secondary photoelectrons: A numerical model, *Ann. Geophys., 7*, 83–90, 1989.

Lindinger, W., F. C. Fehsenfeld, A. L. Schmeltekopf, and E. E. Ferguson, Temperature dependence of some ionospheric ion-neutral reactions from 300°–900°K, *J. Geophys. Res., 79*, 4753–4756, 1974.

Link, R., Dayside magnetospheric cleft auroral processes, Ph.D. thesis, 489 pp., York Univ., Toronto, 1982.

McFarland, M., D. L. Albritton, F. C. Fehsenfeld, E. E. Ferguson, and A. L. Schmeltekopf, Flow-drift technique for ion mobility and ion-molecule reaction rate constant measurements, 2, Positive ion reactions of N^+, O^+, and N_2^+ with O_2 and O^+ with N_2 from thermal to ~2 eV, *J. Chem. Phys., 59*, 6620–6628, 1973.

McFarland, M., D. L. Albritton, F. C. Fehsenfeld, E. E. Ferguson, and A. L. Schmeltekopf, Energy dependence and branching ratio of the $N_2^+ + O$ reaction, *J. Geophys. Res., 79*, 2925–2926, 1974.

Mehr, F. J., and M. A. Biondi, Electron temperature dependence of recombination of O_2^+ and N_2^+ ions with electrons, *Phys. Rev., 181*, 264–271, 1969.

Nagy, A. F., and P. M. Banks, Photoelectron fluxes in the ionosphere, *J. Geophys. Res., 75*, 6260–6270, 1970.

Neupert, W. M., W. E. Behring, and J. C. Lindsay, The solar spectrum from 50 Å to 400 Å, *Space Res. IV*, 719–729, 1964.

Nusinov, A. A., Dependence of the intensity of lines of short-wavelength solar radiation on the solar activity level, *Geomagn. Aeron., 24*, 439–444, 1984.

Ogawa, H. S. and D. L. Judge, Absolute solar flux measurement shortward of 575 Å, *J. Geophys. Res., 91*, 7089–7092, 1986.

Ogawa, H. S., L. R. Canfield, D. McMullin, and D. L. Judge, Sounding rocket measurement of the absolute solar EUV flux utilizing a silicon photodiode, *J. Geophys. Res., 95*, 4291–4295, 1990.

Rees, M. H., *Physics and Chemistry of the Upper Atmosphere*, 289 pp., Cambridge University Press, New York, 1989.

Richards, P. G., and D. G. Torr, An investigation of the consistency of the ionospheric measurements of the photoelectron flux and solar EUV flux, *J. Geophys. Res., 89*, 5625–5635, 1984.

Richards, P. G., and D. G. Torr, Ratios of photoelectron to EUV ionization rates for aeronomic studies, *J. Geophys. Res., 93*, 4060–4066, 1988.

Roble, R. G., and E. C. Ridley, An auroral model for the NCAR thermospheric general circulation model (TGCM), *Ann. Geophys., 5A*, 369–382, 1987.

Rusch, D. W., D. G. Torr, P. B. Hays, and J. C. G. Walker, The O II (7319–7330 Å) dayglow, *J. Geophys. Res., 82*, 719–722, 1977.

Samson, J. A. R., and P. N. Pareek, Absolute photoionization cross sections of atomic oxygen, *Phys. Rev. A, 31*, 1470–1476, 1985.

Schmidtke, G., K. Rawer, H. Botzek, D. Norbert, and K. Holzer, Solar EUV photon fluxes measured aboard Aeros A, *J. Geophys. Res., 82*, 2423–2427, 1977.

Solomon, S. C., and V. J. Abreu, The 630 nm dayglow, *J. Geophys. Res., 94*, 6817–6824, 1989.

Solomon, S. C., P. B. Hays, and V. J. Abreu, The auroral 6300 Å emission: Observations and modeling, *J. Geophys. Res., 93*, 9867–9882, 1988.

Stewart, A. I., and T. E. Cravens, Diurnal and seasonal effects in the *E* region low-latitude nitric oxide, *J. Geophys. Res., 83*, 2453–2456, 1978.

St. Maurice, J.-P., and D. G. Torr, Nonthermal rate coefficients in the ionosphere: The reactions of O^+ with N_2, O_2, and NO, *J. Geophys. Res., 83*, 969–977, 1978.

Timothy, A. F., and J. G. Timothy, Long-term variations in the solar helium II - Lyman alpha line, *J. Geophys. Res., 75*, 6950–6958, 1970.

Titheridge, J. E., An approximate form for the Chapman grazing incidence function, *J. Atmos. Terr. Phys., 50*, 699–701, 1988.

Tobiska, W. K., A Solar Extreme Ultraviolet Flux Model, Ph.D. thesis, Dep. of Aerosp. Eng., Univ. of Colo., Boulder, 1988.

Tobiska, W. K., Revised solar extreme ultraviolet flux model, *J. Atmos. Terr. Phys., 53*, 1005–1018, 1991.

Tobiska, W. K., and C. A. Barth, A solar EUV flux model, *J. Geophys. Res., 95*, 8243–8251, 1990.

Torr, D. G., The photochemistry of the upper atmosphere, in *The Photochemistry of Atmospheres*, edited by J. S. Levine, pp. 165–278, Academic, San Diego, Calif., 1985.

Torr, D. G., and M. R. Torr, Determination of the thermal rate coefficient, products, and branching ratios for the reaction of $O^+(^2D)$ with N_2, *J. Geophys. Res., 85*, 783–787, 1980.

Torr, D. G., M. R. Torr, J. C. G. Walker, A. O. Nier, L. H. Brace, and H. C. Brinton, Recombination of O_2^+ in the ionosphere, *J. Geophys. Res., 81*, 5578–5580, 1976.

Torr, D. G., P. G. Richards, and M. R. Torr, Photochemistry of the ionosphere, in *World Ionosphere Thermosphere Study WITS Handbook Vol. 1*, edited by C. H. Liu and B. Edwards, pp. 1–38, SCOSTEP Secretariat, Urbana, Ill., 1988.

Torr, M. R., and D. G. Torr, Recombination of NO^+ in the mid-latitude trough and the polar ionization hole, *J. Geophys. Res., 84*, 4316–4320, 1979.

Torr, M. R., and D. G. Torr, Ionization frequencies for solar cycle 21: Revised, *J. Geophys. Res., 90*, 6675–6678, 1985.

Torr, M. R., D. G. Torr, and R. A. Ong, Ionization frequencies for major thermospheric constituents as a function of solar cycle 21, *Geophys. Res. Lett., 6*, 771–774, 1979.

Van Tassel, R. A., W. J. McMahon, and L. Heroux, Rocket data of solar EUV flux, thermospheric electron flux, and N_2 second-positive airglow emission, *Environ. Res. Pap., 737, AFGL-TR-81-011*, Air Force Geophys. Lab., Hanscom Air Force Base, Mass., 1981.

Waldteufel, P., Combined incoherent scatter F_1-region observations, *J. Geophys. Res., 76*, 6995–6999, 1971.

Walls, F. L., and G. H. Dunn, Measurement of total cross sections for electron recombination with NO^+ and O_2^+ using ion storage techniques, *J. Geophys. Res., 79*, 1911–1915, 1974.

Woodgate, B. E., D. E. Knight, R. Uribe, P. Sheather, J. Bowles, and R. Nettleship, Extreme ultraviolet line intensities from the Sun, *Proc. R. Soc. London Ser. A, 332*, 291–309, 1973.

Woods, T. N., and G. J. Rottman, Solar EUV irradiance derived from a sounding rocket experiment on November 10, 1988, *J. Geophys. Res., 95*, 6227–6236, 1990.

M. J. Buonsanto, Haystack Observatory, Massachusetts Institute of Technology, Westford, MA 01886.

S. C. Solomon, Laboratory for Atmospheric and Space Physics, University of Colorado, Boulder, CO 80309.

W. K. Tobiska, Jet Propulsion Laboratory, Pasadena, CA 91109.

(Received October 11, 1991;
revised January 24, 1992;
accepted March 24, 1992.)